IEEE Access
Multidisciplinary | Rapid Review | Open Access Journal

Received 13 December 2023, accepted 8 January 2024, date of publication 11 January 2024, date of current version 22 January 2024.

Digital Object Identifier 10.1109/ACCESS.2024.3352636

RESEARCH ARTICLE

Coupling Estimation and Maximum Efficiency Tracking in Multi-Transmitters WPT for Fast Moving Receiver

SHAHID ALI KHAN AND DUKJU AHN
Department of Electrical Engineering, Incheon National University, Incheon 22012, South Korea
Corresponding author: Dukju Ahn (dahn2@inu.ac.kr)

This work was supported in part by Incheon National University under Grant 2020-0434, and in part by the National Research Foundation of Korea under Grant 2022R1F1A1062679.

ABSTRACT Maximum efficiency tracking (MET) with multiple concurrently-activated transmitters (TXs) has not yet been investigated thoroughly. This paper proposes a fast real-time estimation of coupling coefficients and load resistance for multiple concurrently-activated TXs and a moving RX. This is the first paper that demonstrates iteration-less, fast, communication-less MET with power regulation when the RX is moving across multiple activated TX array. The controller senses only the voltage magnitude of TX coil-capacitor resonator, and the input DC voltage and DC current of inverter. Once the parameters are estimated, the controller sets the converters to maximum efficiency point immediately. The benefits of proposed method are that it does not require a communication channel, extra circuit components for MET, time-consuming iterations and computations, and periodic interruption of power flow due to load disconnection or initialization, all of which were limitations in typical methods. Experimental results show that the proposed method provides a fast response (3.8ms) for an RX moving at 6.84 km/h across multiple TXs.

INDEX TERMS Dynamic wireless power transfer, resonant converter, maximum efficiency point tracking, multiple transmitters.

I. INTRODUCTION

In dynamic wireless charging, movement of the RX coil at fast speed has significant impact on the magnetic coupling (k) between TXs and RX, which causes power losses [1]. Maximum efficiency tracking (MET) for multiple-transmitter environment is crucial in dynamic wireless charging to mitigate the losses caused by the misalignment. The challenge of MET in multiple TXs is that, it is essential to not only optimize the load impedance as per traditional single-TX MET, but also adjust the current ratio between multiple concurrently-active TXs according to the TXs-RX coupling ratio [2], [3], [4].

Table 1 and Fig. 1 compare various methods. Existing MET methods either involve the use of TX-RX communication channel, complex calculations at TX or RX side, extra passive power elements, or limited to receiver side control. Fast tracking speed is paramount for dynamic wireless power transfer, as it allows for the RX to move while still maintaining efficient power transfer [5]. Perturbation and observation (P&O) is the most simplistic method [6], [7] that involves small adjustment to the input power, which are then observed to determine the maximum efficiency point (MEP). However, this method suffers from slow speed due to a large number of iterations [8], [9], [10], [11], [12], [13] such as several hundred milliseconds or several seconds. Other techniques and their drawbacks are discussed in Section II and Table 1.

In this paper, we propose a fast real-time estimation of coupling coefficients and load resistance for simultaneously-activated multiple TXs and a moving RX. The proposed method, unlike [5] and [9], does not require the rectifier voltage of the RX for estimating coupling, nor does it

The associate editor coordinating the review of this manuscript and approving it for publication was Harikrishnan Ramiah.

TABLE 1. Comparison with prior works.

Works	Relies on Slow P&O Iteration?	Requires Comm. Channel?	Requires Additional Circuit Component?	Needs more Calculation time?	Power Interruption Due to Load Disconnection or Frequency Sweep?	Failure of Power Regulation due to MET load change	Limited to Single TX Only?	Speed (msec)
[8]	X	X	O	X	X	O	O	0.07~0.6
[10]-[12]	O	X	X	X	X	X	O	~1000 [12]
[14]-[21], [40]	X	O	X	X	X	X	O	~1000[14]
[30],[31]	X	X	X	O	X	O	O	~60000 [30]
[34]	X	X	X	O	X	X	O	n/a
[37]	X	X	X	X	X	O	O	n/a
[35]	X	X	O	X	X	O	O	n/a
[36]	X	O	O	X	X	X	O	47
[39]	X	X	X	X	O	X	O	n/a
[38], [39]	X	X	X	X	O	O	O	62 [38]
[9]	O	X	X	X	X	X	X	~500
[5]	X	O	X	X	X	X	X	10
[22], [41]	X	O	X	X	X	O	X	n/a
This work	**X**	**X**	**X**	**X**	**X**	**X**	**X**	**3.8**

rely on the slow P&O method. Instead, the proposed method can estimate the coupling coefficients and load resistance from TXs side parameters only. Based on the estimation result, the TXs current ratios (i.e., $|\mathbf{I_{TX,1}}|$: $|\mathbf{I_{TX,2}}|$: $|\mathbf{I_{TX,N}}| = k_1$: k_2: k_N) and the RX load impedance are set to MET condition.

According to Table 1 and Fig. 1, our proposed method provides a fast response, eliminates the need of additional power components, complex calculations that take long time, and communication channels. Moreover, there is no initialization or load connection/disconnection steps that periodically pause the power flow. The proposed work can be extended to arbitrary number of transmitters.

II. LIMITATIONS OF PRIOR TECHNIQUES

A. DEPENDENCE ON COMMUNICATION

Another method to implement MET is to extract the k by sensing RX side information and sending it back to TX side via communication channel [5], [14], [15], [16], [17], [18], [19], [20], [21], [22]. Communication is used also in Qi specification where the RX does not move.

However, the backscatter modulation communication of Qi standard is hard to be used in high-power and low-coupling application as in our paper, because these conditions necessitate high modulation depth (i.e. detuning of RX or power dissipation in modulation resistance) which leads to higher loss. Moreover, the backscattering from a traveling RX to multiple TX coils is not yet verified. Also, RF communications cannot be used for dynamic wireless power transfer where the RX moves over a long distances. Typical coverage of Bluetooth is at most ~10 m, and this would be worsen due to the high-power magnetic field noise in WPT. Now, with the moving speed of 6.84 km/h in our paper, the maximum time that the RX can maintain connection with a certain Bluetooth access point is just 5.3 sec. After the 5.3 sec, the communication is lost and the RX should establish a new connection

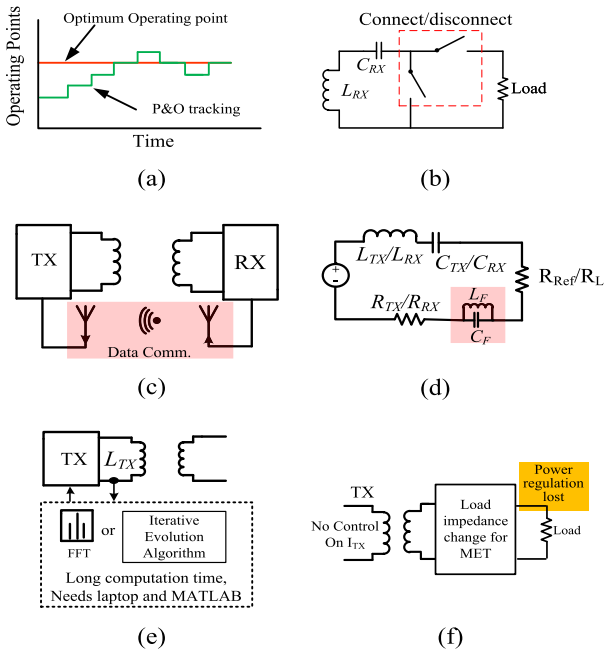

FIGURE 1. Existing approaches for MET. (a) P&O method [9], [10], [11], [12]. (b) Multiple operating modes method [38], [39]. (c) TX-RX communication channel method [14], [15], [16], [17], [18], [19], [20], [21]. (d) Additional circuit components required [8], [34] and [37]. (e) With long computation time [30], [31], [32], [33]. (f) Absence of load power regulation [8], [30], [31], [35], [37], [38].

to another Bluetooth access point. This changeover of connection takes at least 300 msec to 7 sec [23]. During that time, the communication and MET control would be disabled. In summary, when the RX moves at 6.84 km/h speed, the communication is lost per every 5.3 sec and the duration of disconnection can be a few seconds. This is the main reason why the communication is hard to be used for traveling RX unlike existing stationary applications. Additionally, the use of multiple access points results in cost and frequent handovers, resulting in added delays, packet loss [24], [25].

Moreover, interference between multiple access points is common and can also affect the reliability of the system [26]. Also, communication-related delays (at least ∼10msec) can lead to reduced closed-loop performance in [26].

Works in [14] and [16] require communication channel for MET and rectifier voltage regulation. Preregulaltion method for MET in [19] also relies on communication channel. The method in [5] proposes MET which adjusts each TX coil's current to obtain the highest efficiency. For this purpose, rectified voltage and current information of RX is sent to TX-side controller via WiFi channel [5]. The [22] employs the concept of beamforming to steer the magnetic field towards the receiver. The receiver has to communicate its load information back to the transmitter using Bluetooth or in-band communication.

Z-parameter estimation is used in [27], [28], and [29]. However, these parameter estimations require knowledge of the RX side. For example, the [27] and [29]'s TX controller requires the received voltage, and the receiver coil current and load impedance, respectively. Therefore, a communication channel was assumed in [27], [28], and [29]. The drawback of communication channel for the traveling RX has been discussed earlier in this introduction. All these methods of [27], [28], and [29] did not aim the moving RX, and did not prove using a working physical hardware.

B. EXTRA CIRCUITS, DATA, AND COMPUTATION TIME

Some traditional methods used extra data other than the fundamental frequency voltage/current information. In [8] and [21], harmonic frequency components were utilized to estimate k. However, high order harmonic has very low resolution at loosely coupled region ($k < 0.2$). The variation of coupling cannot be distinguished by observing the current information at such region [21]. Another approach proposed in [30] involves frequency sweep monitoring using simple estimation equations. Nevertheless, the accuracy of these methods reduces when leakage inductance of TX coil is not adequately compensated. In [31], a two-layer adaptive differential evolution algorithm is adopted for k estimation without knowing the resonator parameters. Average estimation time of [31] is typically in tens of seconds which is not suitable for dynamic wireless charging. Study in [32] estimates k and load resistance based on amplitude and phase shift of resonant voltage and current. This is challenging in practical scenario because small error in phase sensing can lead to wrong estimation of both unknown parameters. In [33], k estimation is proposed using envelope frequency of the TX coil current during transient, which is complex and cannot be implemented in runtime demonstration. Front-end monitoring proposed in [34] is only valid if the switching frequency is different from resonant frequency of the receiver.

Some works [35], [36] rely on additional passive elements to determine k. The load and k estimation method proposed in [35] requires additional switches and capacitors at TX side. This is at the expense of additional power loss, cost, and volume.

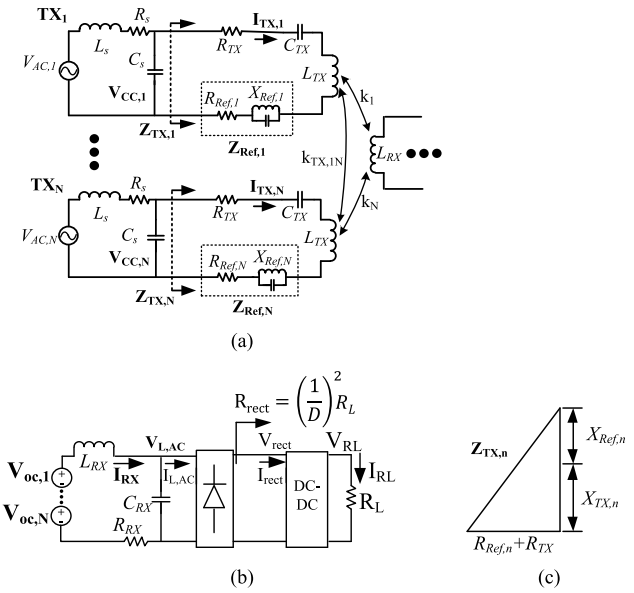

FIGURE 2. (a) Equivalent circuit. $Z_{Ref,n}$ is reflected impedance from RX. $Z_{Ref,n}$ does not physically present in circuit. (b) Equivalent model of RX coupled with multiple TXs. (c) Impedance triangle of TX_n coil coupled with RX.

C. POWER REGULATION FAILURE

Some approaches [8], [18], [37] solely employ MET controller at the receiver side. However, these systems fail to maintain constant load power regulation since the RX load impedance is modified by the RX converter while the TX coil current remains constant. The dc/dc converter in MET serves as impedance transformer, not a voltage regulator. The optimum load must be transformed from actual load via dc/dc converter action. Now, during the impedance transformation of dc/dc converter, the output voltage of dc/dc converter becomes different from the target regulation voltage. According to [11, eq(20)] and referring to Fig. 2(b) of our paper, the impedance transformation relation is $R_{rect} = (1/D)^2 R_L$ where D is the duty cycle of dc/dc converter. The D should be set such that the R_{rect} is transformed to the maximum efficiency load. Therefore, this resultant D value does not regulate output voltage. In other words, the D value for maximum efficiency load transformation and the D value for output voltage regulation are different each other. Therefore, the actual voltage regulation requires TX control.

For example, in [37], the calculation procedure was straightforward; however, it requires the TX input power to remain constant for k estimation at the RX side, regardless of the variation in k during runtime. Consequently, the load voltage is not kept constant. In [18], in order for the TX-side controller to perform the estimation, the RX-side load value must be known to the TX controller. Similarly, for estimation at the RX-side, the voltage across the TX-side source must be known to the RX controller. Since the load keeps changing in practical scenario, communication channel is essential in such methods to update the new load value for k estimation and load voltage regulation.

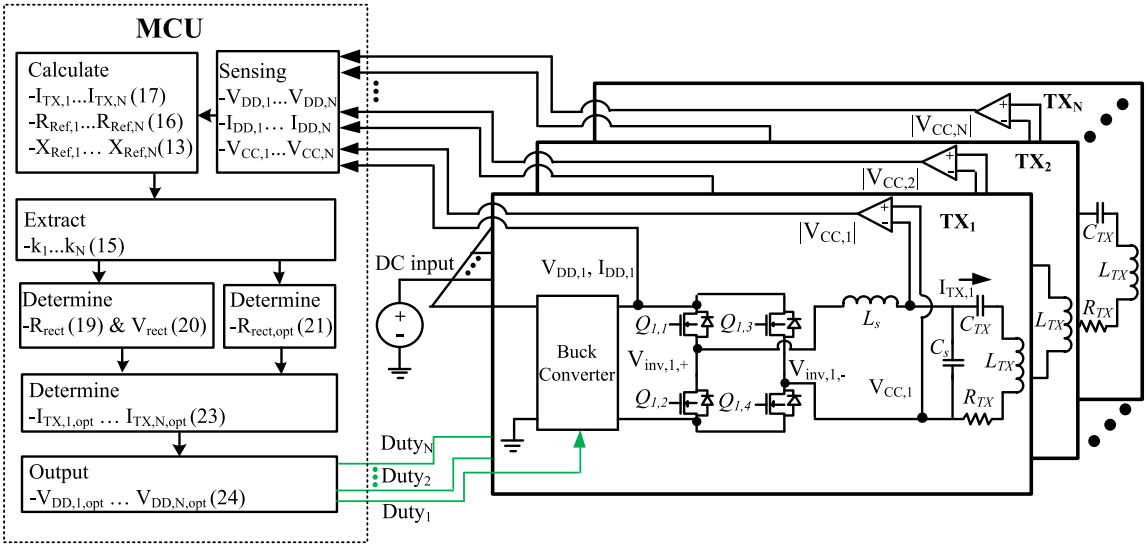

FIGURE 3. Block diagram of proposed method.

D. INTERRUPTION OF POWER

Methods in [38] and [39] determine k by briefly short circuiting the rectifier's output. The underlying strategy is that multiple equations can be obtained by reconfiguring into various circuit topologies and frequencies through the open-circuiting and short-circuiting of load. These multiple equations allow the identification of k. Despotović et al. [26] proposed multiple operating modes (open circuit of secondary side, short circuit of secondary side and load connection) to estimate k and load resistance. The methods proposed in [38] and [39] can perform fast k estimation (62ms and 7ms, respectively) by momentarily shorting the rectifier outputs to ground and performing a frequency sweep. However, these approaches interrupt the continuous flow of power, and are not suitable for dynamic wireless charging because whenever the coupling changes, the load disconnection must be repeated again.

E. EXISTING WORKS FOR MULTIPLE TXS

All the aforementioned coupling estimation methods are for single TX case, and cannot be extended to multiple TXs scenario. The governing equation for the multiple-TX wireless charging system is modified to $\mathbf{V_{RXOUT}} = j\omega M_1\mathbf{I_1} + j\omega M_2\mathbf{I_2} + \ldots + j\omega M_N\mathbf{I}_N$. Even if the TX-side controller is notified of the RX-side rectified output via communication channel, it is not possible to uniquely determine the M_1, $M_2 \ldots M_N$. Similarly, RX-side estimation controller faces the ambiguity problem because the RX load voltage is affected by multiple TX currents and couplings. Whereas the total summation (i.e. RX load voltage) is easily known, individual weight (i.e. individual coupling) cannot be uniquely determined. This necessitates new method to determine $M_1 \ldots M_N$ uniquely.

Until now, there have been some works specifically addressing multiple TX system. In [5], the TX controller must be aware of the rectifier voltage and current for coupling estimation. While this method is effective, it introduces additional complexity and delay due to its reliance on Wi-Fi communication, as discussed earlier in this section. The method in [9] achieves MET in a two-step process without estimating the coupling coefficients. Initially, it equalizes the reflected resistances of all TXs to track the coupling coefficient ratio, and then adjusts the strength of the TXs' current by scaling it up or down to find the optimum load value. This approach takes several hundred milliseconds to converge to the MEP. Both [5] and [9] aim to facilitate a moving RX. However, [9] suffers from a slow response speed, and [5] will struggle with frequent handovers of WiFi access over long distances, which will not be able to facilitate the high-speed, long-distance moving RX. This highlights the need for a fast, communication-less method that can eliminate these issues. Meanwhile, the work in [41] utilizes multiple transmitters to control the direction and magnitude of the magnetic field. This strategy maximizes power by adjusting the ratios between TX coil currents while constraining the magnetic field. However, it does not have the ability to estimate the load impedance. Therefore, the power regulation at receiver cannot be achieved. Even if the [41] maximizes power per given magnetic field strength, it is not the maximum efficiency tracking which requires the transformation of load impedance to optimal value. The [41] is for stationary RX and its control speed is unknown.

III. COUPLING EXTRACTION IN MULTIPLE TXS SCENARIO AND MAXIMUM EFFICIEINCY TRACKING

A. COUPLING ESTIMATION

Employing a parallel resonant receiver provides the advantage of constant current charging at the RX load. Fig. 2 shows a single parallel resonant RX coupled with multiple TXs represented by $k_1, k_2 \ldots k_N$. The $|\mathbf{I_{TX,1}}|, |\mathbf{I_{TX,2}}|, \ldots, |\mathbf{I_{TX,N}}|$ are

the TX coil currents. The L_s and C_s are part of LCC resonant inverter network. L_{RX} is the self-inductance of receiver coil and C_{RX} is the receiver's resonant capacitor. By applying first harmonic approximation, the open circuit voltage $\mathbf{V_{ocT}}$ induced at the RX by each coupled TX can be summed and written as:

$$\mathbf{V_{ocT}} = -j\omega\sqrt{L_{RX}}(k_1\sqrt{L_{TX}}\mathbf{I_{TX,1}} + k_2\sqrt{L_{TX}}\mathbf{I_{TX,2}} +, \cdots, +k_N\sqrt{L_{TX}}\mathbf{I_{TX,N}}) \quad (1)$$

$$\mathbf{V_{L,AC}} = \frac{-j\mathbf{V_{ocT}}R_{L,AC}}{\omega L_{RX}} \quad (2)$$

$\mathbf{V_{L,AC}}$ is the rectifier input voltage [42], ω is the angular frequency, and $R_{L,AC}$ is the rectifier input impedance seen by the RX coil which is $R_{L,AC} = \frac{\pi^2}{8}R_{rect}$ for parallel resonant RX. Bold denotes complex quantity with real and imaginary part. Referring to Fig. 2(b), induced $\mathbf{I_{RX}}$ can be found from the $\mathbf{V_{ocT}}$ and $\mathbf{V_{L,AC}}$ as

Referring to Fig. 2(a), total input impedance seen by the TX_n is $\mathbf{Z_{TX,n}}$ which can be written as

$$\mathbf{Z_{TX,n}} = R_{TX} + jX_{TX} + \sum_{m=1,m\neq n}^{N} j\omega k_{TX,nm}L_{TX}\frac{\mathbf{I_{TX,m}}}{\mathbf{I_{TX,n}}} + \mathbf{Z_{Ref,n}} \quad (5)$$

Here, R_{TX} is the parasitic resistance of the TX_n coil, X_{TX} is the TX self-impedance which is $\omega L_{TX} - \frac{1}{\omega C_{TX}}$. Overlapped TX coils structure is used in this paper to eliminate the TX-TX cross coupling ($k_{TX,nm} = 0$). $\mathbf{Z_{Ref,n}}$ is the total reflected impedance of n*th* TX which is

$$\mathbf{Z_{Ref,n}} = j\omega k_n\sqrt{L_{TX}L_{RX}}\frac{\mathbf{I_{RX}}}{\mathbf{I_{TX,n}}} \quad (6)$$

Substituting (4), as shown at the bottom of the next page into (6) to determine the total reflected impedance induced at n*th* TX gives

$$\mathbf{Z_{Ref,n}} = \left(-1 - \frac{jR_{L,AC}}{\omega L_{RX}}\right) \times \left(j\omega k_n^2 L_{TX} + \sum_{m=1,m\neq n}^{N} j\omega k_n k_m L_{TX}\left|\frac{\mathbf{I_{TX,m}}}{\mathbf{I_{TX,n}}}\right|\right) \quad (7)$$

The (7) can be rearranged to real and imaginary part as

$$R_{Ref,n} = \frac{\omega k_n^2 L_{TX}R_{L,AC}}{\omega L_{RX}} + \sum_{m=1,m\neq n}^{N}\frac{\omega k_n k_m L_{TX}R_{L,AC}}{\omega L_{RX}}\left|\frac{\mathbf{I_{TX,m}}}{\mathbf{I_{TX,n}}}\right| \quad (8)$$

$$jX_{Ref,n} = -j\omega k_n^2 L_{TX} - \sum_{m=1,m\neq n}^{N} j\omega k_n k_m L_{TX}\left|\frac{\mathbf{I_{TX,m}}}{\mathbf{I_{TX,n}}}\right| \quad (9)$$

$R_{Ref,n}$ is the real part of the $\mathbf{Z_{Ref,n}}$ that states the actual power transferred to RX. Meanwhile, $jX_{Ref,n}$ is the imaginary part of $\mathbf{Z_{Ref,n}}$ which can be used to determine the magnetic coupling coefficients since it is independent of $R_{L,AC}$. Solving (9) for k_n yields

$$k_n = \sqrt{\frac{X_{Ref,n}}{\omega L_{TX}\left(1 + \sum_{m=1,m\neq n}^{N}\frac{X_{Ref,m}}{X_{Ref,n}}\left|\frac{\mathbf{I_{TX,m}}}{\mathbf{I_{TX,n}}}\right|^2\right)}} \quad (10)$$

From Fig. 2(a), the total impedance seen by *n*th TX coil is

$$\left|\mathbf{Z_{TX,n}}\right| = \frac{\left|\mathbf{V_{CC,n}}\right|}{\left|\mathbf{I_{TX,n}}\right|} \quad (11)$$

Referring to Fig. 2(c), the impedance triangle can be solved as

$$\left|\mathbf{Z_{TX,n}}\right|^2 = \left(X_{Ref,n} + X_{TX,n}\right)^2 + \left(R_{Ref,n} + R_{TX}\right)^2 \quad (12)$$

Combining (11) and (12), the $jX_{Ref,n}$ induced at TX_n can be runtime measured as

$$X_{Ref,n} = \sqrt{\left(\left(\frac{\left|\mathbf{V_{CC,n}}\right|}{\left|\mathbf{I_{TX,n}}\right|}\right)^2 - \left(R_{Ref,n} + R_{TX}\right)^2\right)} - X_{TX} \quad (13)$$

Using (10) and (13), k_n can be uniquely determined as follows

$$k_n = \sqrt{\frac{\sqrt{\left(\left(\frac{\left|\mathbf{V_{CC,n}}\right|}{\left|\mathbf{I_{TX,n}}\right|}\right)^2 - \left(R_{Ref,n} + R_{TX}\right)^2\right)} - X_{TX}}{\omega L_{TX}\left(1 + \sum_{m=1,m\neq n}^{N}\frac{X_{Ref,m}}{X_{Ref,n}}\left|\frac{\mathbf{I_{TX,m}}}{\mathbf{I_{TX,n}}}\right|^2\right)}} \quad (14)$$

From (8) and (9), it is evident that the ratios of the real part of the total reflected impedance are mathematically equal to the ratios of imaginary part (i.e., $R_{Ref,1}$:$R_{Ref,2}$: $R_{Ref,N} = X_{Ref,1}$: $X_{Ref,2}$: $X_{Ref,N}$). Consequently, (14) can be also expressed as

$$k_n = \sqrt{\frac{\sqrt{\left(\left(\frac{\left|\mathbf{V_{CC,n}}\right|}{\left|\mathbf{I_{TX,n}}\right|}\right)^2 - \left(R_{Ref,n} + R_{TX}\right)^2\right)} - X_{TX}}{\omega L_{TX}\left(1 + \sum_{m=1,m\neq n}^{N}\frac{R_{Ref,m}}{R_{Ref,n}}\left|\frac{\mathbf{I_{TX,m}}}{\mathbf{I_{TX,n}}}\right|^2\right)}} \quad (15)$$

where $n = 1, 2, 3, \ldots, N$. $R_{Ref,n}$ has a relation with the input DC resistance of inverter, and can be found as

$$R_{Ref,n} = \frac{\pi^2}{8\left(\omega C_s\right)^2\left(\frac{V_{DD,n}}{I_{DD,n}} - \frac{R_s\pi^2}{8}\right)} - R_{TX} \quad (16)$$

where $V_{DD,n}$ and $I_{DD,n}$ are the DC input voltage and current of *n*th inverter, respectively, which can be easily obtained runtime [5]. The (15) reveals that the proposed method estimates coupling using only transmitter parameters, thereby negating the requirement for communication channels or position sensors.

This paper utilizes LCC resonant inverters due to its constant current source characteristics, and to ensure load independence for the $\mathbf{I_{TX}}$, the parameter $\omega L_S - 1/\omega C_S$

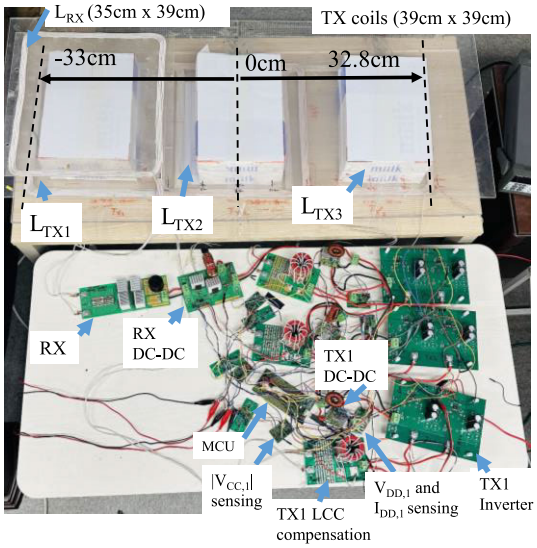

FIGURE 4. Experimental setup with 3 TXs.

TABLE 2. Component parameters.

Parameter	Value	Parameter	Value
L_{TX}	53 µH	R_S	0.1 Ω
R_{TX}	0.2 Ω	C_S	364 nF
C_{TX}	80 nF	L_{RX}	27.5 uH
L_S	10 uH	C_{RX}	127.5nF

has been set to zero [43]. The $\mathbf{I_{TX,n}}$ for each TX can be determined as

$$\mathbf{I_{TX,n}} = -j(4/\pi)\omega C_s V_{DD,n} \tag{17}$$

This indicates that the phase and magnitude of TX current remains unaffected by the variations of L_{TX}–C_{TX}, coil couplings, and reflected impedance [43].

B. RX LOAD AND POWER ESTIMATION WITHIN TX

As discussed in the Section II, the MET in [8], [18], and [37] fail to achieve constant power regulation. This is because the TX side does not have information of the RX power, and therefore $|\mathbf{I_{TX}}|$ could not be adjusted, regardless of the load and coupling variation. Therefore, the TX needs to know RX power for power regulation during MET. While some prior literatures achieve this via wireless data communication or load connection/disconnection interrupts, we do not rely on them due to their limitations discussed in Section II. In this article, the TX can estimate the RX power and load impedance by monitoring TX quantities. Referring to (8), the reflected resistance of nth transmitter is

$$R_{Ref,n} = \frac{jR_{rect}}{\omega L_{RX}}\frac{\pi^2}{8}\left(-j\omega k_n^2 L_{TX} - \sum_{m=1,m\neq n}^{N} j\omega k_n k_m L_{TX}\left|\frac{\mathbf{I_{TX,m}}}{\mathbf{I_{TX,n}}}\right|\right) \tag{18}$$

Rearranging (18) and solving for R_{rect} yields

$$R_{rect} = \frac{8}{\pi^2}\frac{R_{Ref,n}}{\frac{L_{TX}}{L_{RX}}\left(k_n^2 + \sum_{m=1,m\neq n}^{N} k_n k_m\left|\frac{\mathbf{I_{TX,m}}}{\mathbf{I_{TX,n}}}\right|\right)} \tag{19}$$

Here, $k_1, k_2, \ldots, k_N$ are determined using (15), and $R_{Ref,n}$ is calculated using (16). L_{TX} and L_{RX} are already known parameters. Finally, R_{rect}, which represents the total output resistance of the RX rectifier, can be accurately known without the need of any communication channel or load disconnection procedures. The RX rectified voltage is estimated within TX side as

$$V_{rect} = jR_{rect}\sqrt{\frac{L_{TX}}{L_{RX}}}\left(k_1\left|\mathbf{I_{TX,1}}\right| + k_2\left|\mathbf{I_{TX,2}}\right| + , \cdots, + k_N\left|\mathbf{I_{TX,N}}\right|\right) \tag{20}$$

The innovation of (20) and (14) compared to [5], [14], [36], and [20] is that the V_{rect} and k_n are estimated within TX without relying on communication channel. In contrast, the [5], [14], [20], and [36] had to sense the V_{rect} using RX-side hardware and forward the sensed value to TX in order to estimate coupling coefficient. The communication channel cannot be used in dynamic WPT because the RX keeps moving away from the communication access point, which is extensively discussed in Section II-A.

C. MAXIMUM EFFICIENCY TRACKING AND POWER REGULATION FOR MULTIPLE TXs WITHOUT ITERATION OR COMMUNICATION

A simultaneous achievement of MET and power regulation in multiple TX scenario can be realized by fulfilling two main requirements. First, it is necessary to enforce coil current ratios to match the magnetic coupling ratio (i.e., $|\mathbf{I_{TX,1}}|$: $|\mathbf{I_{TX,2}}|$: $|\mathbf{I_{TX,N}}| = k_1$: k_2: k_N). Second requirement is optimizing the overall magnitudes of $\mathbf{I_{TX}}$ in such a way that the R_{Rect} becomes the optimum load impedance $R_{Rect,opt}$, which can be found as

$$R_{rect,opt} = \frac{8}{R_{RX}\pi^2(\omega C_{RX})^2\sqrt{1 + \frac{\omega^2 L_{TX}L_{RX}(k_1^2+k_2^2+,\cdots,+k_N^2)}{R_{TX}R_{RX}}}} \tag{21}$$

$$\mathbf{V_{ocT}} - \mathbf{V_{L,AC}} = j\omega\mathbf{I_{RX}}L_{RX} \tag{3}$$

$$\mathbf{I_{RX}} = \frac{(k_1\sqrt{L_{TX}}\mathbf{I_{TX,1}} + k_2\sqrt{L_{TX}}\mathbf{I_{TX,2}} + , \cdots, + k_N\sqrt{L_{TX}}\mathbf{I_{TX,N}})(-1 - \frac{jR_{L,AC}}{\omega L_{RX}})}{\sqrt{L_{RX}}} \tag{4}$$

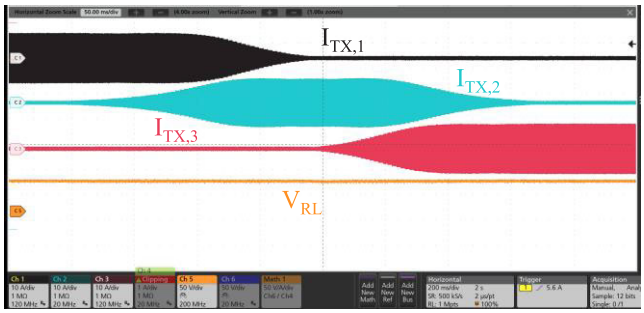

FIGURE 5. $I_{TX,1}$-$I_{TX,3}$ and V_{RL} waveforms when RX is moving from −33cm to 32.8cm at 6.84 km/h velocity ($I_{TX,1}$-$I_{TX,3}$: 10A/div, V_{RL} 50V/div, and time: 50ms/div.)

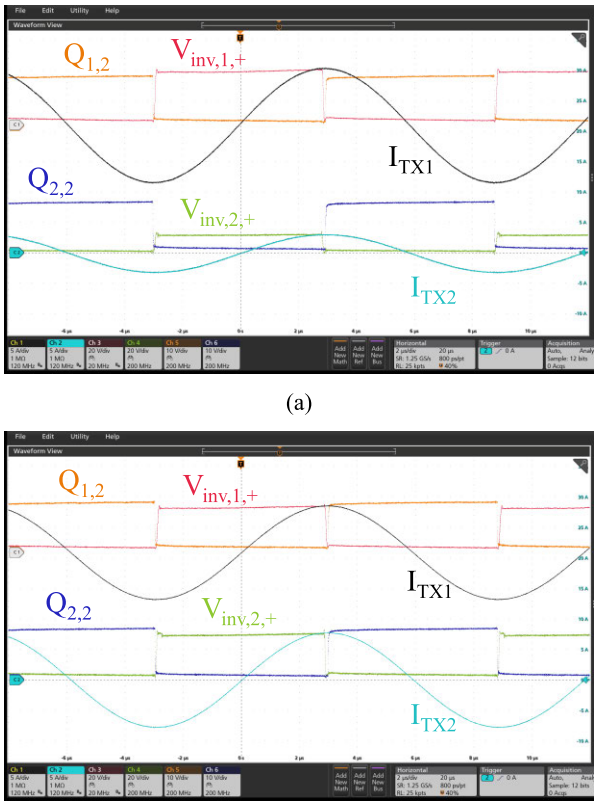

FIGURE 6. Waveforms of TXs coil currents, high-side mosfet's source voltages and low-side mosfet's gate voltages. (a) At RX location −25.2cm. (b) At RX location −16.75cm. ($I_{TX,1}$, $I_{TX,2}$: 5A/div, $V_{inv,1,+}$, $V_{inv,2,+}$: 20V/div, and $Q_{1,2}$, $Q_{2,2}$: 10V/div.)

We seek to achieve both the $R_{rect,opt}$ and power regulation simultaneously. They are achieved at

$$V_{rect,opt} = \sqrt{\frac{R_{rect,opt} V_{rect}^2}{R_{rect}}} \tag{22}$$

Here, R_{rect} and V_{rect} are the runtime estimated RX load status estimated within TX controller using (19)-(20). The benefit of (19)-(22) is that it achieves not only maximum efficiency but also power regulation. This is advantageous compared to [8], [26], and [37]. Specifically, the [8] loses power regulation when RX impedance is adjusted because the TX does not know the RX's load status.

The three conditions – the optimum current ratio ($|\mathbf{I_{TX,1}}|$: $|\mathbf{I_{TX,2}}|$: $|\mathbf{I_{TX,N}}| = k_1$: k_2: k_N), the optimum load impedance ($R_{rect,opt}$), and power regulation – are satisfied simultaneously when $|\mathbf{I_{TX,n}}| = |\mathbf{I_{TX,n,opt}}|$ which is as follows:

$$\left|\mathbf{I_{TX,n,opt}}\right| = \frac{k_n \left(1 + R_{RX}\left((\omega C_{TX})^2 R_{rect,opt}\right)\right)}{\omega\sqrt{L_{TX} L_{RX}}\left(k_1^2 + k_2^2 +, \cdots, +k_N^2\right)} \times \sqrt{\frac{2V_{rect}^2}{(\omega C_{TX})^2 R_{rect,opt} R_{rect}}} \tag{23}$$

The relationship between $|\mathbf{I_{TX,n,opt}}|$ and $V_{DD,n,opt}$ is

$$V_{DD,n,opt} = \frac{\pi}{4}\frac{\left|\mathbf{I_{TX,n,opt}}\right|}{\omega C_s} \tag{24}$$

Fig. 3 summarizes the control of the proposed tracking method. MCU senses $V_{DD,1}$, $V_{DD,2}$,…, $V_{DD,N}$, $I_{DD,1}$, $I_{DD,2}$,…, $I_{DD,N}$, and $|\mathrm{V_{CC,1}}|$, $|\mathrm{V_{CC,2}}|$,…, $|\mathrm{V_{CC,N}}|$. Since LCC resonant inverter's coil current only depends on input voltage, $|\mathbf{I_{TX,1}}|$, $|\mathbf{I_{TX,2}}|$,…, $|\mathbf{I_{TX,N}}|$ is directly determined from the sensed VDDs using (17). $R_{Ref\,1}$, $R_{Ref\,2}$, …$R_{Ref\,,N}$ and $X_{Ref\,,1}$, $X_{Ref\,,2}$, …$X_{Ref\,,N}$ are calculated using (16) and (13), respectively. The extracted coupling values from (15) are then used to determine the RX side power and optimum rectifier resistance $R_{rect,opt}$, which are then further used by (23) to calculate $|\mathbf{I_{TX,1,opt}}|$, $|\mathbf{I_{TX,2,opt}}|$,…, $|\mathbf{I_{TX,N,opt}}|$. The optimum $|\mathbf{I_{TX,n}}|$ obtained from (23) achieves both conditions of MET, which are the current ratios (i.e., $|\mathbf{I_{TX,1}}|$: $|\mathbf{I_{TX,2}}|$: $|\mathbf{I_{TX,N}}| = k_1$: k_2: k_N) and $R_{rect,opt}$, at the constraint of target power regulation. In other words, the $|\mathbf{I_{TX,n}}|$ values specified by (23) enforce the RX DC-DC converter to automatically transform R_{rect} to $R_{rect,opt}$ of (21). A MCU takes only one cycle (3.8ms) from sensing to setting the $|\mathbf{I_{TX,opt}}|$ for all TXs.

D. COMPARISON WITH PRIOR WORKS

Table 1 summarizes the comparison of existing works and proposed work. Fig. 1 shows existing approaches for MET. The works in [14], [15], [16], [17], [18], [19], [20], [21], and [40] employ a DC-DC converter at the receiver side for constant output voltage regulation and MET. As discussed in the previous section, achieving MET requires the TX side to know the k, rectifier's voltage, and rectifier load resistance. This causes additional problems as discussed in Section II-A, II-B, II-C, and II-D. The proposed work avoids such problems and can estimate the TX-RX magnetic coupling, rectifier's output voltage, and load resistance directly from TX side. The proposed method provides a fast MET for multiple concurrently-operating TXs which is suitable for moving RX over wide area. The method is a real time that does not require periodic initialization steps such as load disconnection or frequency sweeping, avoiding interruption of power flow. No additional power components are used.

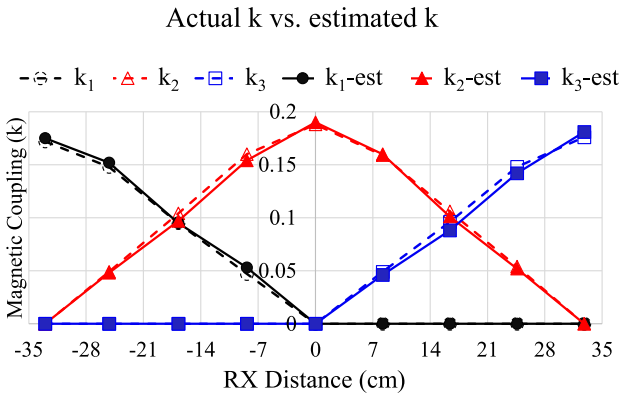

FIGURE 7. Estimated coupling values matches the actual coupling values.

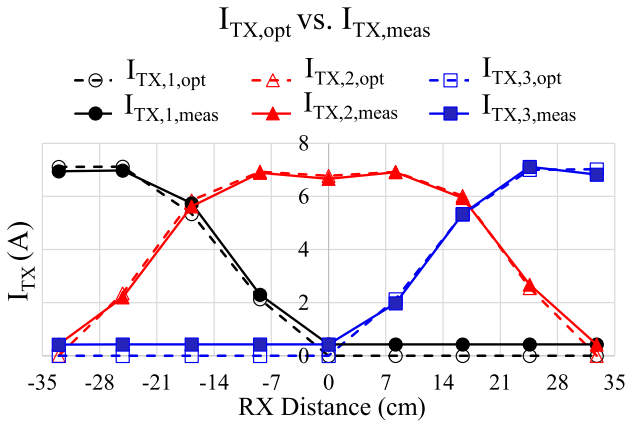

FIGURE 8. $I_{TX,1}$-$I_{TX,3}$ values measured in comparison with calculated $I_{TX,1}$-$I_{TX,3}$ optimum values.

IV. MEASUREMENT

The proposed method is verified by a prototype, which is presented in Fig. 4. The target application for this system is an Automated Guided Vehicle (AGV) used in warehouses or factories. AGVs in warehouse follow a predetermined path and operate continuously, transporting goods from storage to picking/loading stations. The parameters such as dimensions, power, and frequency are chosen for this application. Table 2 and Fig. 4 present the component parameters. The vertical air-gap between TX and RX is 10 cm. The operating frequency of the system is 85 kHz and the load power is 200W. The 85 kHz is a standard for high-power applications [44]. Employing fast dynamic wireless charging eliminates the downtime of AGV for manual replacement/charging of batteries. The proposed system provides uninterrupted power with fast MET, and estimates the coupling solely from TX parameters, which is ideal for the described scenario. RX's moving speed with current system is 6.84 km/h, which is suitable for the target application.

Single MCU TMS320F28335 controls the three TXs. Each inverter is connected to a shared clock from MCU, which eliminates the phase imbalance and switching frequency variations in TXs. TMCS1100A3 is used to sense the DC current

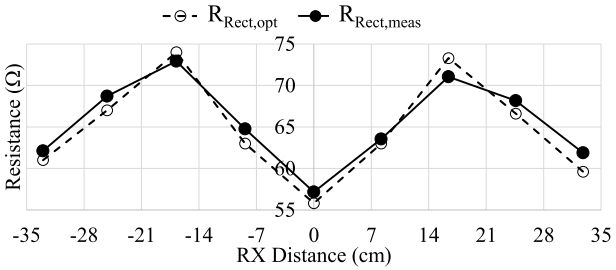

FIGURE 9. Proposed method tracks the $R_{rect,opt}$ that maximizes the overall efficiency.

at inverter's input. $|V_{CC,n}|$ is measured using instrumentation amplifier AD8421 and $|\mathbf{I_{TX,n}}|$ is calculated from the sensed input voltage of inverter. The voltages and current that are used to extract coupling are only sensed at TX side. Therefore, communication channel is not necessary for the proposed method.

Fig. 5 presents the real-time MET tracking when RX is moving from −33 cm to 32.8 cm at a velocity of 6.84 km/h. The RX movement begins at −33 cm, where k_1 is strong and k_2 and k_3 are both zero. Therefore, the magnitude of $\mathbf{I_{TX1}}$ is high, while magnitudes of $\mathbf{I_{TX2}}$ and $\mathbf{I_{TX3}}$ are low. As the RX gradually moves closer to TX_2 and TX_3, the magnitudes of $\mathbf{I_{TX2}}$ and $\mathbf{I_{TX3}}$ increase, while $\mathbf{I_{TX1}}$ decreases gradually according to (23) and (24).

Fig. 6 shows that the TXs maintain zero-voltage switching (ZVS) and in-phase coil current for different RX positions. In order to achieve ZVS in our experiment, the impedances of TXs are set to be inductive. All TXs share a common clock from a single MCU. Due to the constant current nature of LCC inverter as in (17), the coil currents are in-phase each other, irrespective of any variations in reflected impedance and coupling [5], [9], [44].

Fig. 7 shows the coupling values estimated by the proposed method. They coincide with the actual coupling coefficient. Fig. 8 compares the measured coil current values ($I_{TX,meas}$) with theoretically calculated optimum current values ($I_{TX,opt}$). The $I_{TX,meas}$ values at different RX position match those of $I_{TX,opt}$. Fig. 9 presents the tracking accuracy of RX rectifier's optimum output resistance. $R_{Rect,opt}$ trace refers to the theoretically calculated optimum resistance, while $R_{Rect,meas}$ is the measured output resistance in the runtime. The $R_{Rect,meas}$ coincides with the $R_{Rect,opt}$.

Fig. 10 compares the efficiencies of the proposed system with conventional systems. The green triangle trace refers to the activation of only a single TX, in which the TX with the highest coupling is activated while the other TXs are turned off. Due to the lack of MET control, the $|\mathbf{I_{TX}}|$ is fixed to guarantee the required power for the worst-case coupling position (±16.5cm). This $|\mathbf{I_{TX}}|$ is not optimum for efficiency viewpoint of best-case coupling positions (0cm). Specifically, this $\mathbf{I_{TX}}$ magnitude, which is required for worst-case position, is too high for best-coupling case causing unnecessary loss. Therefore, even at best-coupling position, the efficiency of

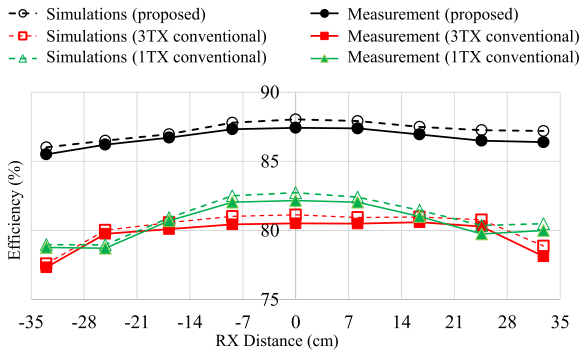

FIGURE 10. Efficiency comparison of conventional system and proposed MET when RX is swept from −33cm to 32.8cm. The I_{TX} level of 1TX conventional setup is chosen to guarantee the required power for the worst-case coupling position.

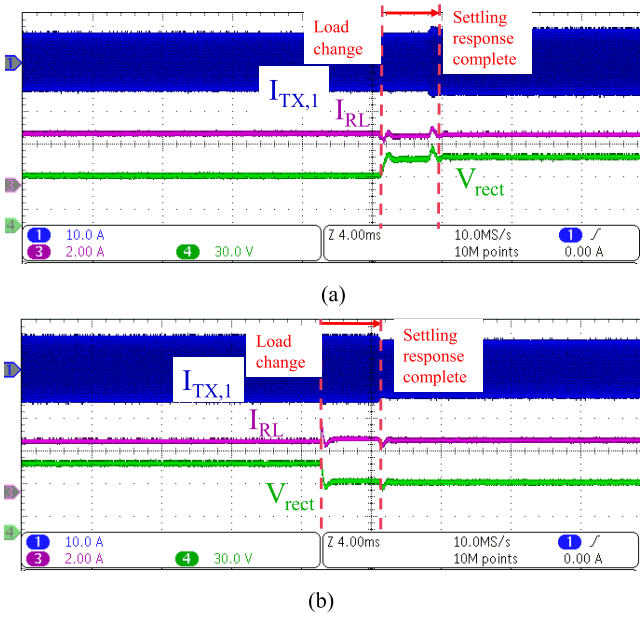

FIGURE 11. Step Change of RX power. MCU adjusts the TX coil current and settles the output in 3.8ms. (a) Load power change from 150W to 200W. ($I_{TX,1}$: 10A/div, I_{RL}: 2A/div, and V_{rect}: 30V/div). (b) Load power change from 200W to 150W.

conventional case becomes low. Red rectangular trace refers to a conventional system where all three TXs are turned on without MET operation. The weakly coupled TXs that do not contribute to power flow are also activated due to the lack of MET operation, which demonstrates the necessity of MET.

On the other hand, the black circle trace of Fig. 10 presents efficiency of the proposed method. The proposed method optimizes the ratio and the magnitudes of $\mathbf{I_{TXs}}$ (Fig. 8) as well as the RX load impedance according to MET requirement. The simulation and measurement agrees well with each other.

Fig. 11 shows the response to step change in load power. TX MCU continuously monitors k_1, k_2, k_3, R_{rect} and V_{rect}. As a change is made, MCU determines new optimum operating point and settles the output in 3.8ms. Constant-current charging is achieved with MET. Table 3 compares the

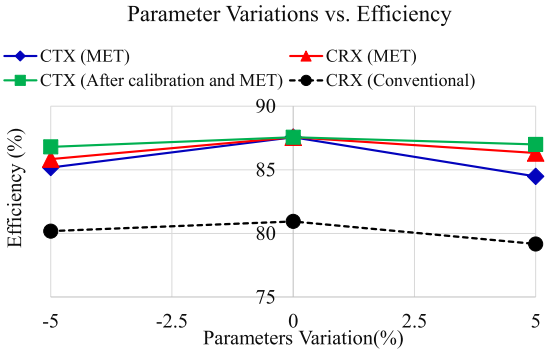

FIGURE 12. Efficiency with parameter uncertainties.

TABLE 3. Comparison of performance between proposed and existing methods.

Works	Efficiency (%)	Coupling (k)	Accuracy (%)	Load Power (W)	Tracking speed (msec)
[8]	63	0.34	~95	27.7	0.07~0.6
[12]	81	0.15	n/a	100	~1000
[14]	85	0.168	~96	~110	~1000
[36]	86	0.168	92%	~65	47
[9]	79	0.11	n/a	478	~500
[5]	78.8	0.165	~96	200	10
This work	**87.4**	**0.19**	**97.9**	**200**	**3.8**

performance of the proposed method with existing methods. The table clearly shows that the proposed system offers the highest efficiency and the most accurate estimation of magnetic coupling with fast speed.

V. CONCLUSION

We propose iteration-less, communication-less, one-cycle calculation MET with power regulation when the RX is moving across multiple simultaneously-activated TX array. It takes only 3.8ms for the MCU to sense the TX side parameters, estimate k_1, k_2, …, k_N and load voltage, then update the $|\mathbf{I_{TXs}}|$ values. The method can maintain maximum efficiency and power regulation condition for the RX moving at 6.84 km/h physical velocity. At this moving speed, the RX travels 0.72 cm per every 3.8 msec where the 3.8 msec is the response time of our controller. Hence, the controller can optimally re-adjust the $I_{TX,(1,2,...N)}$ and efficiency whenever the TX-RX coil misalignment is 0.72 cm. In other words, even though the TX-RX alignment keeps varying during the AGV movement, the controller tracks the maximum efficiency at the spatial resolution of 0.72cm.

Advantages of proposed MET are summarized in Table 1. It does not require data communication, additional circuit components in the middle of power stage, time-consuming iterations and computations, and periodic interruption of power flow due to initialization or load disconnect. It also achieves RX power regulation despite the RX load impedance adjustment. The proposed method estimates the coupling coefficients for multiple simultaneously-operating TXs. The

simplified architecture and cost-effectiveness of the proposed method make it an attractive solution for real world application.

APPENDIX

Fig. 12 presents the simulation results for variations in different parameters. C_{TX}(MET) and C_{RX}(MET) represent the variations of C_{TX} and C_{RX} in the proposed method without any calibration. C_{TX} (After calibration and MET) refers to the proposed method where the C_{TX} is calibrated after parameter variation. Meanwhile, C_{RX} (conventional) refers to the case without MET while the variation of C_{RX} occurs. It is evident that even if the TX side is unaware of the change in C_{RX} or C_{TX}, the efficiency is not significantly affected by parameter variations.

To improve the efficiency for parameter variation, the controller can periodically recalibrate, such as once a day, to check whether C_{TX} has deviated to a different value. During standby (i.e. the coupling between TX,n and RX is zero), the (12) and Fig. 2(a) indicate that $\left|\mathbf{Z_{TX,n}}\right|^2 = \left(X_{TX,n}\right)^2 + \left(R_{TX}\right)^2 \cong \left(X_{TX,n}\right)^2$. Here, the $\mathbf{Z_{TX,n}}$ is monitored by sensor as in Fig. 3 and (11). This allows us to determine and update $X_{TX,n}$ even if the C_{TX} varies over time. The square green trace of Fig. 12 is the situation where the recalibration is used. It shows that the recalibration minimizes the degradation of efficiency for the parameter variation.

REFERENCES

[1] S. A. Khan and D. Ahn, "Phase synchronization and magnitude control with interference between transmitters in wireless power transfer," *IEEE J. Emerg. Sel. Topics Power Electron.*, vol. 11, no. 4, pp. 4526–4535, Aug. 2023, doi: 10.1109/JESTPE.2022.3210520.

[2] P. K. S. Jayathurathnage, A. Alphones, D. M. Vilathgamuwa, and A. Ong, "Optimum transmitter current distribution for dynamic wireless power transfer with segmented array," *IEEE Trans. Microw. Theory Techn.*, vol. 66, no. 1, pp. 346–356, Jan. 2018, doi: 10.1109/TMTT.2017.2698460.

[3] S. Huh and D. Ahn, "Two-transmitter wireless power transfer with optimal activation and current selection of transmitters," *IEEE Trans. Power Electron.*, vol. 33, no. 6, pp. 4957–4967, Jun. 2018, doi: 10.1109/TPEL.2017.2725281.

[4] C. Zhang, D. Lin, and S. Y. R. Hu, "Efficiency optimization method of inductive coupling wireless power transfer system with multiple transmitters and single receiver," in *Proc. IEEE Energy Convers. Congr. Expo. (ECCE)*, Milwaukee, WI, USA, Sep. 2016, pp. 1–6, doi: 10.1109/ECCE.2016.7855071.

[5] D.-H. Kim, S. Kim, S.-W. Kim, J. Moon, I. Cho, and D. Ahn, "Coupling extraction and maximum efficiency tracking for multiple concurrent transmitters in dynamic wireless charging," *IEEE Trans. Power Electron.*, vol. 35, no. 8, pp. 7853–7862, Aug. 2020, doi: 10.1109/TPEL.2019.2962203.

[6] D. Bui, T. M. Mostafa, A. P. Hu, and R. Hattori, "DC–DC converter based impedance matching for maximum power transfer of CPT system with high efficiency," in *Proc. IEEE PELS Workshop Emerg. Technol., Wireless Power Transf. (Wow)*, Jun. 2018, pp. 1–5, doi: 10.1109/WOW.2018.8450929.

[7] J. Li, D. Xu, and D. Wang, "Perturb and observe method of impedance matching for magnetically coupled wireless power transfer system," in *Proc. Chin. Autom. Congr. (CAC)*, Nov. 2018, pp. 2513–2517, doi: 10.1109/CAC.2018.8623452.

[8] J. Hu, J. Zhao, and F. Gao, "A real-time maximum efficiency tracking for wireless power transfer systems based on harmonic-informatization," *IEEE Trans. Power Electron.*, vol. 38, no. 1, pp. 1275–1287, Jan. 2023, doi: 10.1109/TPEL.2022.3200096.

[9] D.-H. Kim and D. Ahn, "Maximum efficiency point tracking for multiple-transmitter wireless power transfer," *IEEE Trans. Power Electron.*, vol. 35, no. 11, pp. 11391–11400, Nov. 2020, doi: 10.1109/TPEL.2019.2919293.

[10] M. Fu, H. Yin, X. Zhu, and C. Ma, "Analysis and tracking of optimal load in wireless power transfer systems," *IEEE Trans. Power Electron.*, vol. 30, no. 7, pp. 3952–3963, Jul. 2015, doi: 10.1109/TPEL.2014.2347071.

[11] W. X. Zhong and S. Y. R. Hui, "Maximum energy efficiency tracking for wireless power transfer systems," *IEEE Trans. Power Electron.*, vol. 30, no. 7, pp. 4025–4034, Jul. 2015, doi: 10.1109/TPEL.2014.2351496.

[12] Z. Li, K. Song, J. Jiang, and C. Zhu, "Constant current charging and maximum efficiency tracking control scheme for supercapacitor wireless charging," *IEEE Trans. Power Electron.*, vol. 33, no. 10, pp. 9088–9100, Oct. 2018, doi: 10.1109/TPEL.2018.2793312.

[13] D. Patil, M. Sirico, L. Gu, and B. Fahimi, "Maximum efficiency tracking in wireless power transfer for battery charger: Phase shift and frequency control," in *Proc. IEEE Energy Convers. Congress Expo.*, Sep. 2016, pp. 1–8, doi: 10.1109/ECCE.2016.7855234.

[14] X. Dai, X. Li, Y. Li, and A. P. Hu, "Maximum efficiency tracking for wireless power transfer systems with dynamic coupling coefficient estimation," *IEEE Trans. Power Electron.*, vol. 33, no. 6, pp. 5005–5015, Jun. 2018, doi: 10.1109/TPEL.2017.2729083.

[15] J. M. Miller, O. C. Onar, and M. Chinthavali, "Primary-side power flow control of wireless power transfer for electric vehicle charging," *IEEE J. Emerg. Sel. Topics Power Electron.*, vol. 3, no. 1, pp. 147–162, Mar. 2015, doi: 10.1109/JESTPE.2014.2382569.

[16] X. Hu, Y. Wang, Y. Jiang, W. Lei, and X. Dong, "Maximum efficiency tracking for dynamic wireless power transfer system using LCC compensation topology," in *Proc. IEEE Energy Convers. Congr. Expo. (ECCE)*, Sep. 2018, pp. 1992–1996, doi: 10.1109/ECCE.2018.8557494.

[17] W. Zhong and S. Y. R. Hui, "Maximum energy efficiency operation of series-series resonant wireless power transfer systems using on-off keying modulation," *IEEE Trans. Power Electron.*, vol. 33, no. 4, pp. 3595–3603, Apr. 2018, doi: 10.1109/TPEL.2017.2709341.

[18] V. Jiwariyavej, T. Imura, and Y. Hori, "Coupling coefficients estimation of wireless power transfer system via magnetic resonance coupling using information from either side of the system," *IEEE J. Emerg. Sel. Topics Power Electron.*, vol. 3, no. 1, pp. 191–200, Mar. 2015, doi: 10.1109/JESTPE.2014.2332056.

[19] H. Li, J. Li, K. Wang, W. Chen, and X. Yang, "A maximum efficiency point tracking control scheme for wireless power transfer systems using magnetic resonant coupling," *IEEE Trans. Power Electron.*, vol. 30, no. 7, pp. 3998–4008, Jul. 2015, doi: 10.1109/TPEL.2014.2349534.

[20] Z. Huang, S.-C. Wong, and C. K. Tse, "Control design for optimizing efficiency in inductive power transfer systems," *IEEE Trans. Power Electron.*, vol. 33, no. 5, pp. 4523–4534, May 2018, doi: 10.1109/TPEL.2017.2724039.

[21] J. Hu, J. Zhao, and C. Cui, "A wide charging range wireless power transfer control system with harmonic current to estimate the coupling coefficient," *IEEE Trans. Power Electron.*, vol. 36, no. 5, pp. 5082–5094, May 2021, doi: 10.1109/TPEL.2020.3032659.

[22] J. Jadidian and D. Katabi, "Magnetic MIMO," in *Proc. 20th Annu. Int. Conf. Mobile Comput. Netw.*, Sep. 2014.

[23] R. A. Gheorghiu, V. Iordache, and A. C. Cormos, "Analysis of handshake time for Bluetooth communications to be implemented in vehicular environments," in *Proc. 40th Int. Conf. Telecommun. Signal Process. (TSP)*, Barcelona, Spain, Jul. 2017, pp. 144–147, doi: 10.1109/TSP.2017.8075955.

[24] Z. Chen, Z. Luo, X. Duan, and L. Zhang, "Terminal handover in software-defined WLANs," *EURASIP J. Wireless Commun. Netw.*, vol. 2020, no. 1, Dec. 2020, doi: 10.1186/s13638-020-01681-w.

[25] A. A. Mansour, N. Enneya, M. Ouadou, and D. Aboutajdine, "Handoff between Wimax and WiFi networks," in *Proc. 2nd Int. Conf. Innov. Comput. Technol. (INTECH)*, Casablanca, Morocco, Sep. 2012, pp. 69–74, doi: 10.1109/INTECH.2012.6457767.

[26] Ž. Despotovic, D. Reljic, V. Vasic, and D. Oros, "Steady-state multiple parameters estimation of the inductive power transfer system," *IEEE Access*, vol. 10, pp. 46878–46894, 2022, doi: 10.1109/ACCESS.2022.3170913.

[27] D. Kobuchi, J. Ahn, Y. Narusue, and H. Morikawa, "Z-parameter estimation for multiple-input multiple-output wireless power transfer systems via a phase retrieval method," in *Proc. Wireless Power Week (WPW)*, Bordeaux, France, Jul. 2022, pp. 313–317, doi: 10.1109/WPW54272.2022.9853866.

[28] G. Yang, M. R. V. Moghadam, and R. Zhang, "Magnetic MIMO signal processing and optimization for wireless power transfer," *IEEE Trans. Signal Process.*, vol. 65, no. 11, pp. 2860–2874, Jun. 2017, doi: 10.1109/TSP.2017.2673816.
[29] T. Aoki, Q. Yuan, D. Quang-Thang, M. Okada, and H.-M. Hsu, "Maximum transfer efficiency of MIMO-WPT system," in *Proc. IEEE Wireless Power Transf. Conf. (WPTC)*, Montreal, QC, Canada, Jun. 2018, pp. 1–3, doi: 10.1109/WPT.2018.8639417.
[30] Y. Yang, Y. Jiang, S.-C. Tan, and S. R. Hui, "A frequency-sweep based load monitoring method for weakly-coupled series-series compensated wireless power transfer systems," in *Proc. IEEE PELS Workshop Emerg. Technol., Wireless Power Transf. (Wow)*, Jun. 2018, pp. 1–5, doi: 10.1109/WoW.2018.8450907.
[31] Y. Yang, S.-C. Tan, and S. Y. R. Hui, "Front-end parameter monitoring method based on two-layer adaptive differential evolution for SS-compensated wireless power transfer systems," *IEEE Trans. Ind. Informat.*, vol. 15, no. 11, pp. 6101–6113, Nov. 2019, doi: 10.1109/TII.2019.2924926.
[32] J. P. W. Chow and H. S. H. Chung, "Use of primary-side information to perform online estimation of the secondary-side information and mutual inductance in wireless inductive link," in *Proc. IEEE Appl. Power Electron. Conf. Expo. (APEC)*, Mar. 2015, pp. 2648–2655, doi: 10.1109/APEC.2015.7104725.
[33] A. Lusiewicz, J. Noeren, M. Jaksch, and N. Parspour, "A novel method for online coupling factor determination in inductive power transfer systems," in *Proc. IEEE Wireless Power Transf. Conf. (WPTC)*, Jun. 2018, pp. 1–4, doi: 10.1109/WPT.2018.8639460.
[34] J. Yin, D. Lin, T. Parisini, and S. Y. Hui, "Front-end monitoring of the mutual inductance and load resistance in a series–series compensated wireless power transfer system," *IEEE Trans. Power Electron.*, vol. 31, no. 10, pp. 7339–7352, Oct. 2016, doi: 10.1109/TPEL.2015.2509962.
[35] Y.-G. Su, H.-Y. Zhang, Z.-H. Wang, A. P. Hu, L. Chen, and Y. Sun, "Steady-state load identification method of inductive power transfer system based on switching capacitors," *IEEE Trans. Power Electron.*, vol. 30, no. 11, pp. 6349–6355, Nov. 2015, doi: 10.1109/TPEL.2015.2411755.
[36] Y. Liu and H. Feng, "Maximum efficiency tracking control method for WPT system based on dynamic coupling coefficient identification and impedance matching network," *IEEE J. Emerg. Sel. Topics Power Electron.*, vol. 8, no. 4, pp. 3633–3643, Dec. 2020, doi: 10.1109/JESTPE.2019.2935219.
[37] H. Nawada, Y. Takahashi, K. Hata, T. Imura, H. Fujimoto, Y. Hori, and T. Yabumoto, "Coupling coefficient estimation for wireless power transfer system at constant input power operation," in *Proc. IEEE PELS Workshop Emerg. Technologies: Wireless Power Transf. (WoW)*, Jun. 2019, pp. 288–291, doi: 10.1109/WoW45936.2019.9030621.
[38] Y. Yang, S. C. Tan, and S. Y. R. Hui, "Fast hardware approach to determining mutual coupling of series–series-compensated wireless power transfer systems with active rectifiers," *IEEE Trans. Power Electron.*, vol. 35, no. 10, pp. 11026–11038, Oct. 2020, doi: 10.1109/TPEL.2020.2977140.
[39] J. Zeng, S. Chen, Y. Yang, and S. Y. R. Hui, "A primary-side method for ultrafast determination of mutual coupling coefficient in milliseconds for wireless power transfer systems," *IEEE Trans. Power Electron.*, vol. 37, no. 12, pp. 15706–15716, Dec. 2022, doi: 10.1109/TPEL.2022.3188288.
[40] Qi Wireless Power Consortium, "The qi wireless power transfer system, power class 0 specification, parts 1 and 2: Interface definitions," *Wireless Power Consortium*, pp. 43–46, Apr. 2016.
[41] X. Tian, K. T. Chau, W. Liu, H. Pang, and C. H. T. Lee, "Maximum power tracking for magnetic field editing-based omnidirectional wireless power transfer," *IEEE Trans. Power Electron.*, vol. 37, no. 10, pp. 12901–12912, Oct. 2022, doi: 10.1109/TPEL.2022.3178097.
[42] B. Lee and D. Ahn, "Robust self-regulated rectifier for parallel-resonant rx coil in multiple-receiver wireless power transmission system," *IEEE J. Emerg. Sel. Topics Power Electron.*, vol. 9, no. 3, pp. 3812–3821, Jun. 2021, doi: 10.1109/JESTPE.2019.2929279.
[43] Z. Pantic, S. Bai, and S. M. Lukic, "ZCS LCC-compensated resonant inverter for Inductive-Power-Transfer application," *IEEE Trans. Ind. Electron.*, vol. 58, no. 8, pp. 3500–3510, Aug. 2011, doi: 10.1109/TIE.2010.2081954.
[44] *System Reference Document (SRdoc); Wireless Power Transmission (WPT) Systems Operating Below 30 MHz*. Accessed: Jul. 1, 2023. [Online]. Available: https://www.etsi.org/deliver/etsi_tr/103400_103499/103493/01.01.01_60/tr_103493v010101p.pdf

SHAHID ALI KHAN received the B.S. degree in electrical (computer) engineering from COMSATS University Islamabad (Abbotabad Campus), Pakistan, in 2016, and the M.S. degree in electrical engineering from Incheon National University, Incheon, South Korea, where he is currently pursuing the Ph.D. degree in electrical engineering.

His current research interests include power electronics for wireless power transfer and analog/RF integrated circuit design.

DUKJU AHN received the B.S. degree in electrical engineering from Seoul National University, Seoul, South Korea, in 2007, and the M.S. and Ph.D. degrees in electrical engineering from the Korea Advanced Institute of Science and Technology (KAIST), Daejeon, South Korea, in 2010 and 2012, respectively.

He is currently with Incheon National University, Incheon, South Korea. He was a recipient of the 2020 Second Prize Paper Award from IEEE TRANSACTIONS ON POWER ELECTRONICS.